Biogeosciences
Open Access
Discussions

Peru upwelling plankton respiration: calculations of carbon flux, nutrient retention efficiency and heterotrophic energy production

T. T. Packard[1], N. Osma[1], I. Fernández-Urruzola[1], L. A. Codispoti[2], J. P. Christensen[3], and M. Gómez[1]

[1]Marine Ecophysiology Group (EOMAR), Universidad de Las Palmas de Gran Canaria, Campus Tafira, 35017 Las Palmas de Gran Canaria, Spain
[2]Horn Point Laboratory, University of Maryland, 21613-0775 Cambridge Maryland, USA
[3]Green Eyes LLC, Easton, MD 21601, USA

Correspondence to: T. T. Packard (theodoretrainpackard@gmail.com)

Abstract

Oceanic depth profiles of plankton respiration are described by a power function, $R_{CO_2} = (R_{CO_2})_0(z/z_0)^b$ similar to the vertical carbon flux profile. Furthermore, because both ocean processes are closely related, conceptually and mathematically, each can
5 be calculated from the other. The exponent (b), always negative, defines the maximum curvature of the respiration depth-profile and controls the carbon flux. When b is large, the C flux (F_C) from the epipelagic ocean is low and the nutrient retention efficiency (NRE) is high allowing these waters to maintain high productivity. The opposite occurs when b is small. This means that the attenuation of respiration in ocean water columns
10 is critical in understanding and predicting both vertical F_C as well as the capacity of epipelagic ecosystems to retain their nutrients. The NRE is a new metric defined as the ratio of nutrient regeneration in a seawater layer to the nutrients introduced into that layer via F_C. A depth-profile of F_C is the integral of water column respiration. This relationship facilitates calculating ocean sections of F_C from water column respiration.
15 In a F_C section across the Peru upwelling system we found a F_C maximum extending down to 400 m, 50 km off the Peru coast. Finally, coupling respiratory electron transport system activity to heterotrophic oxidative phosphorylation promoted the calculation of an ocean section of heterotrophic energy production (HEP). It ranged from 250 to 500 J d^{-1} m^{-3} in the euphotic zone, to less than 5 J d^{-1} m^{-3} below 200 m on this ocean
20 section.

1   Introduction

Respiration is as ubiquitous in the ocean as are the microorganisms that cause it. It is controlled by the respiratory electron transport (ETS) activity in eukaryotic mitochondria and prokaryotic cell membranes, is responsible for the bulk of oceanic
25 O$_2$ consumption, and is coupled to oceanic CO$_2$ production, heterotrophic energy production, and organic C degradation. Even in anoxic seawater it produces CO$_2$

while reducing nitrogen oxides to N_2 or SO_4^{-2} to H_2S. Plankton respiration is a key variable in calculating net primary productivity (Ducklow and Doney, 2013) in developing oceanic C models, in resolving the autotrophic-heterotrophic states of ocean ecosystems (Williams et al., 2012), and in understanding vertical ocean F_C rates

5 (Giering et al., 2014). The research team led by Sarah Giering (Giering et al., 2014) demonstrated that, contrary to previous efforts (Burd et al., 2010), but in accord with classical oceanographic understanding (Suess, 1980), zooplankton and microplankton (prokaryot) respiration balance vertical carbon flux. This finding supports the use of plankton respiration in assessing vertical F_C in the ocean water column. Conceptually,

10 the reciprocal relationship between water column respiration and F_C, from the ocean's epipelagic zone, is clear (Suess, 1980). However, describing this reciprocal relationship mathematically, as a function of ocean depth in the forms,

$$R = f(z) \text{ and } F_C = \int_{z_1}^{z_2} R \, dz$$

was delayed until the helium-tritium studies of Jenkins, the sediment trap studies of

15 VERTEX program, and respiratory electron transport system (ETS) measurements in the Gulf of Maine (Packard and Christensen, 2004). In the later, microplankton ETS measurements were used to build power function models of respiratory CO_2 production (R_{CO_2}) and F_C. Here, we extend this approach to calculate a microplankton respiration section across the Peru Upwelling System (Tables 2 and 3, and Fig. 2a) and to model

20 F_C on this transect (Figs. 1a and 2b, Table 2). We focused our measurements on microplankton because its biomass dominates ocean water columns (Laufkötter et al., 2013). The section was made at a time of regime-change when the Peru upwelling system and the El Niño-Southern Oscillation (ENSO) underwent a shift (Santoso et al., 2013). Here we document some of the biological phenomena that occurred at that

25 time. With the F_C and the R_{CO_2} models we calculate the nutrient retention efficiency (Packard and Gómez, 2013; Osma et al., 2014), a new metric that quantifies the

Full Screen / Esc

ability of an ocean layer to retain its nutrients (Fig. 2c). Conceptually, the nutrient retention efficiency (NRE) is the nutrient remineralization rate within an ocean layer normalized by nutrients entering that layer via C flux. Below the euphotic zone it can be calculated as the inverse of the F_C transfer efficiency (Buesseler et al., 2007; Buesseler and Boyd, 2009), but we show here that it can also be calculated from a profile of plankton respiration. In addition, using different limits to the F_C integration we calculate the sum of the benthic respiration and C burial (Fig. 3a) that occurs on the sea floor. Finally we use the respiration models and the couple between ETS activity and oxidative phosphorylation to calculate light-independent heterotrophic energy flow (Karl, 2014). This energy is generated in the form of ATP by ATP synthase, an enzyme motor coupled to a heterotrophic respiratory process such as O_2 utilization or NO_3^- reduction (Watt et al., 2010; Ferguson, 2010). In all types of respiration, the ATP synthase senses the pH and EMF (electromotive force) gradient across the membrane in which the ATP synthase is embedded (Lane et al., 2010) and when the gradient is sufficiently strong ($\sim 225\,\mathrm{mV}$), the rotor of the ATP synthase starts its rotary production of ATP (Walker, 1998). Heterotrophic ATP generation in any ecosystem is largely based on exploiting the Gibbs Free Energy (ΔG) released during the oxidation of different organic compounds. The biochemistry of ATP and the ETS was unknown in 1925, but even then the idea of capturing biologically useable energy from respiration (R) was appreciated by Lotka (Lotka, 1925). A generation later Odum built on this concept to describe energy flow in fresh water streams (Odum, 1956). Building on this earlier work, Karl recently argued that biological energy production in the ocean should be assessed to provide insight to variability in ocean productivity (Karl, 2014). Here, we address his concern by calculating HEP in a C-Line section (Fig. 2d). This HEP is the energy produced while ATP is generated by respiratory O_2 consumption (R_{O_2}) in the microplankton community composed of phytoplankton, bacteria, archea, and protozoans in the epipelagic layer and by the R_{O_2} and NO_3^- reduction in microbial communities of bacteria, archea, and protozoans in the meso- and bathypelagic waters of the Peru Current upwelling system.

2   Methods

2.1   Research site

The site of this CUEA investigation at 15° S off Pisco Peru (Fig. 1) was chosen because the upwelling is strong, persistent, and well known (Wooster, 1961; Fernández et al.,
2009). It was the focus of the R/V *Anton Bruun* cruise 15 (Ryther et al., 1971), the R/V *T.G. Thompson Pisco* expedition in 1969 (Barber et al., 1978), and others (Wyrtki, 1967) before it was the focus of the CUEA-JOINT II program of which the JASON Expedition was a part (King, 1981; Richards, 1981). However, in spite of the many previous expeditions to this site most of them took place in the austral fall (March-April-
May). The JASON-76 expedition was unique because it took place in the late winter and austral spring (August-September-October-November) when the southeast trade winds would be at their strongest (Wooster, 1961). In this way it was thought that the results might be more comparable with results from upwelling studies made in the Northern Hemisphere's spring-time upwelling off NW Africa. The results presented here are from
the 10 to 24 September leg of JASON-76 on board Duke University's Oceanographic ship, R/V *Eastward*, cruise number, E-5H-67 (Packard and Jones, 1978).

2.2   Hydrographic and productivity sampling

All sampling was conducted along the C-Line (Fig. 1a) that extended seaward from the coast at position C1, just south of Cabo Nazca (Pisco), across the deep trench
to position C14, 185 km offshore (Packard, 1981). Hydrographic sections were made at the beginning of the expedition (10–11 September) and again after a lapse of 10 days (20–21 September). The endpoint coordinates were from $15°3.2'$ S, $75°26.0'$ W to $15°55.8'$ S, $75°31.4'$ W (Packard and Jones, 1978; Kogelshatz et al., 1978). In addition, between 10 and 24 September, productivity stations, that focused on the
biological properties at depths at which the light was 100, 50, 30, 15, 5, 1, and 0.1 % of the surface incident radiation (light-depths), were made at C-Line positions Packard

and Jones (1978). Each morning before 10:00 LT casts were made with 30 L Niskin PVC bottles to 6 light-depths (1, 5, 15, 30, 50, and 100 %). Each Niskin bottle was flushed at depth in yo-yo fashion both by the action of the ship's roll and by meter oscillations with the winch. On deck it was drained immediately, without prefiltration,

5 into a well rinsed carboy for subsampling and returned to depth for the next sample. The six samples were taken within an hour. Subsamples were drawn for phytoplankton productivity, inorganic nutrient salts, (ammonium, reactive phosphorus, NO_3^-, NO_2^- and silicate), ETS and NO_3^- reductase activities, and particulate protein (Packard and Jones, 1978). Station coordinates are given in Table 1. The inorganic nutrient salts,

10 salinity, temperature, and O_2 can be found in CUEA data reports 38 and 45 (Hafferty et al., 1978; Kogelshatz et al., 1978). Chlorophyll, and phytoplankton productivity (^{14}C-uptake) are reported in CUEA data report (Barber et al., 1978). The ^{14}C-uptake data were calculated on an hourly basis (Table 1) from the 24 h-productivity data (Kogelshatz et al., 1978). Light was measured as daily total solar radiation with an Eppley Model

15 8–48 pyranometer placed above the ship's bridge (Packard and Jones, 1978).

2.3 ETS activity, respiratory O_2 consumption, CO_2 production, and NO_3^- reduction

Respiratory ETS activity in the Ez was measured according to Kenner and Ahmed (1975) and in deeper waters, according to Packard et al. (1971). Potential R and

20 R were calculated from ETS activity according to Packard and Christensen (2004). Since microbial respiratory NO_3^- reduction to nitrogen gas (denitrification) occurs in the water column between 47 and 400 m between positions C3 to C12 (Garfield et al., 1979; Codispoti and Packard, 1980) (Table 2; Fig. 2a), calculations of R_{CO_2} in these waters from the ETS activity measurements differ from those in oxic waters that

25 support aerobic respiration. The calculation of in vivo denitrification rates (R_{N_2}) is from Codispoti and Packard (1980) according to Codispoti et al. (2001). The approach has recently been corroborated by Dalsgaard et al. (2012). R_{CO_2} was calculated as $R_{CO_2} =$

$[106/60 \, \text{mol} \, C \, (\text{mol} \, N_2)^{-1} \times \text{ETS activity} \, (\text{mol} \, e^- \, h^{-1} \, m^{-3})]/[105 \, \text{mol} \, e^- \, (\text{mol} \, N_2)^{-1}]$ using the C–N conversion of Gruber and Sarmiento (1997).

2.4 R modelling

To generate R models as depth functions, the ETS-based R was plotted against depths
5 normalized by the depth of the R maximum (z_m) (Packard and Christensen, 2004). From these plots power functions of the form, $R = R_m(z/z_m)^b$ were fitted to the data using Sigma Plot (version 12.5) according to Charland (2002). These R models at each station were used to create Fig. 2a. Note that R in the Ez of these sections is based directly on the ETS measurements while the R in the aphotic zone below is
10 based on the R models in Table 4.

2.5 F_C, NRE, and HEP calculations

The F_C was calculated from depth-normalized water column R (Packard and Christensen, 2004; Packard and Gómez, 2013; Osma et al., 2014). However, here, only the F_C associated with the microplankton is calculated. The planktonic R_{CO_2} in
15 a seawater cube is considered as equivalent to the difference between the F_{C_1} through the top of the cube and F_{C_2} through the bottom of the cube and assuming that DOC-based R and lateral POC flux, compared to F_C, are negligible (Craig, 1971), one can write an expression, $R_{CO_2} = F_{C_1} - F_{C_2}$. In other words, in the vertical, one-dimensional case, the changes in the F_C between depths in a water column are equal to the R_{CO_2}
20 between those depths. Extrapolating this conceptual model to the deep ocean water column, using continuous mathematics, and assuming seafloor C burial small, the F_C into the top of a water column (F_{C_t}) can be calculated by integrating all the R below the

top boundary (z_t) to the ocean bottom (z_s).

$$F_{C_t} = \int_{z_t}^{z_s} R_{CO_2} \, dz \tag{1}$$

All F_C calculations here are based on depth-normalized power functions of R ($R_{CO_2} = R_m(z/z_m)^b$, Table 3). For the C flux (F_{f-s}) through any depth layer in the water column
5 (z_f) down to z_s, we use Eq. (2) and its integrated version in Eq. (3).

$$F_{f-s} = \int_{z_f}^{z_s} R_{CO_2} \, dz = \int_{z_f}^{z_s} R_m \, (z/z_m)^b \, dz \tag{2}$$

$$F_{f-s} = \left\{ R_m / \left[(b+1) z_m^b \right] \right\} \left(z_s^{b+1} - z_f^{b+1} \right) \tag{3}$$

Note that z_f is any depth between z_t and z_s ($z_t \leqslant z_f \leqslant z_s$) and F_{f-s} is associated with the microplankton respiration.
10 NRE is equal the R ($\text{mol CO}_2 \, \text{d}^{-1} \, \text{m}^{-3}$) within an ocean layer divided by the depth-integrated F_C ($\text{mol C d}^{-1} \, \text{m}^{-3}$) into the volume of that layer expressed as a %. Since the Redfield N/C or P/C ratio is applied to both parts of the ratio, they cancel leaving the ratio unitless. NRE is also the inverse of the transfer efficiency through the same layer (Packard and Gómez, 2013). For Fig. 2c it was calculated for 20 m layers below the Ez
15 to the ocean bottom from the R models in Table 4 and the F_C models in Table 6.

HEP (Fig. 2d) was calculated from R_{O_2} and R_{N_2}, both derived from the ETS measurements, or from the modeled R_{O_2}, or R_{N_2}. For oxic seawater HEP = 2 × 2.5 × 48 × R_{O_2} where 2 represents the number of electron pairs required to reduce O_2 to $2H_2O$, 2.5 represents the ATP/2e$^-$ ratio (Ferguson, 2010), 48 is the ΔG in
20 J mmol^{-1} of ATP (Alberty and Goldberg, 1992; Moran et al., 2012), and R_{O_2} in the respiratory O_2 consumption rate as mmol $O_2 \, \text{d}^{-1} \, \text{m}^{-3}$. For NO$_3^-$ R in anoxic waters

$HEP = 5 \times 1.0 \times 48 \times R_{N_2}$, where 5 is the number of electron pairs required to reduce NO_3 to N_2, 1.0 is the $ATP/2e^-$ ratio (van Loosdrecht et al., 1997; Smolders et al., 1994), 48 is the ΔG as before, and R_{N_2} in the respiratory NO_3^- reduction rate as $mmol\,N_2\,d^{-1}\,m^{-3}$.

3 Ocean setting

Oceanographic properties (Table 1) on a C-Line transect at 15° S across the Peru Current upwelling system (Fig. 1a) in middle September of the ENSO transition year, 1976, were measured on the R/V *Eastward* during the JASON-76 cruise of the Coastal Upwelling Ecosystem Analysis (CUEA) JOINT-II expedition. Upwelling was evident during this period. Seawater density (σ_t) and NO_3^- sloped surfaceward close to the coast (Fig. 1b). From 25 m (σ_t) rose from 26.0 to 26.1 and NO_3^- rose from 12 to 16 µM. As these dense nutrient-rich waters rose, fertilized the sunlit surface waters at the upwelling center (C3), and flowed offshore towards C5 and C8, phytoplankton bloomed to $7\,mg\,m^{-3}$ chlorophyll *a* and $18\,mg\,C\,h^{-1}\,m^{-3}$ of productivity (Table 1 and Fig. 1b). The dynamics of this process could be seen in the variability of the euphotic zone (Ez) depth. It ranged, from a low of 21 m at C5, the biomass and metabolism maximum position, to twice the depth, 43 m, at the offshore position, C14 (Table 1). Temporal variability was exemplified at the trench position (C12) where over a week, the Ez depth decreased from 40 to 21 m. Minimal variability occurred at position C8, where over 6 days, the Ez depth remained at 29 m (Table 1). In general, a shallow Ez is caused by high plankton biomass with a high potential for metabolism, and contrary conditions associated with a deep Ez.

4 Results

Sea surface R_{O_2} ranged six-fold from a low of $24.1\,\mu mol\,O_2\,m^{-3}\,h^{-1}$ at the upwelling center to a high of $144.7\,\mu mol\,O_2\,m^{-3}\,h^{-1}$, 93 km offshore at the trench position,

C12 (Table 1). Within days, R_{O_2} could change 3-fold both inshore and offshore (Table 3). During the week between C3 stations 15 and 21, R_{O_2} rose from 24.1 to 84.0 $\mu mol\,O_2\,m^{-3}\,h^{-1}$ and R_{O_2} at C12 rose from 47.1 $\mu mol\,O_2\,m^{-3}\,h^{-1}$ (station 17) to 144.7 $\mu mol\,O_2\,m^{-3}\,h^{-1}$ (station 35, Table 2). This high respiration (R) at station (sta) 35,

5 occurred in a diatom bloom of *Chaetoceros compressus* and *Ch. lorenzianus*. Such temporal variability in seawater R_{O_2} is just beginning to be documented (Fernández-Urruzola et al., 2014; Osma et al., 2014). Similar increases were seen in the chlorophyll and net productivity at C3 and C12 (Table 1). The co-occurrence of this rise in R_{O_2}, chlorophyll and net productivity suggests seawater R_{O_2} being driven by phytoplankton.

10 Below the sea surface, microplankton R_{O_2} usually increased to a subsurface maximum within the Ez and then decreased dramatically towards the bottom of the Ez and into the dark ocean below (Tables 2 and S3). In oxic waters R was reported as R_{O_2} in $\mu mol\,O_2\,m^{-3}\,h^{-1}$, but in anoxic, sulfide-free mesopelagic waters containing oxides of nitrogen (Fig. 1b and c), R continued as denitrification (R_{N_2}) (Dalsgaard et al.,

15 2012; Codispoti and Packard, 1980) and was reported in $\mu mol\,N_2\,m^{-3}\,h^{-1}$ (shaded numbers in Table 3). R_{CO_2} (Fig. 2a) was calculated in oxic waters from R_{O_2} considering the Redfield ratio (C/O_2) of 0.71 (Takahashi et al., 1985) and in anoxic waters with NO_3^- respiration, from R_{NO_3} by a Redfield ratio of $60N_2/106CO_2$ (Packard and Christensen, 2004; Codispoti and Packard, 1980). Power functions ($R_{CO_2} = R_m(z/z_m)^b$)

20 were selected for F_C calculations for consistency (Packard and Christensen, 2004; Packard and Codispoti, 2007) and also because they better described the data than logarithmic or exponential functions. The values for R_m and b are given in Table 4. The exponent, b, is always negative. Each station's R model was tested for veracity by plotting the predicted R from the R maximum to the depths below (Table 4). R_{CO_2}

25 (Fig. 2a) ranged in the Ez from 0.4 $mmol\,CO_2\,m^{-3}\,d^{-1}$ in the upwelling center (C3, sta 15) to 3 $mmol\,CO_2\,m^{-3}\,d^{-1}$ at C5, the shelf edge sta 20. The lowest epipelagic R_{CO_2} (Table 5) compares with the R_{CO_2} range of 22–27 $mmol\,CO_2\,m^{-2}\,d^{-1}$ reported

recently in eddy-upwelling in the South China Sea (Jiao et al., 2014). In the denitrifying waters R_{CO_2} was in the µmol range with a low of $4\,\mu mol\,CO_2\,m^{-3}\,d^{-1}$ at C5 (sta 37) to $133\,\mu mol\,CO_2\,m^{-3}\,d^{-1}$ at C3 (sta 21). In the mesopelagic waters below 500 m (Table 5) R_{CO_2} ranged from 0.4 to $6.1\,\mu mol\,CO_2\,m^{-3}\,d^{-1}$ over a week at C-Line position C8, at other locations R_{CO_2} fell in between this range. Deeper in the water column, over the trench and beyond, bathypelagic R_{CO_2} ranged from $0.3\,\mu mol\,CO_2\,m^{-3}\,d^{-1}$ at C10 over the trench to $3.7\,\mu mol\,CO_2\,m^{-3}\,d^{-1}$ at C8 over the continental slope (Table 5). Benthic R_{CO_2} and C burial (Table 5 and Fig. 3a) ranged from a high of $90\,mmol\,CO_2\,m^{-2}\,d^{-1}$ at C3, the upwelling center, to a low of $0.09\,mmol\,CO_2\,m^{-2}\,d^{-1}$ at trench position, C10, with a depth of 4300 m. The R_{CO_2} section in Fig. 2a show clearly the strength of R and its associated remineralization in the upper 50 m of the water column and a tongue of high R descending deeper into the water column at position C8, 50 km off the coast. F_C along the C-Line transect is shown in Fig. 2b. In order to include the inshore stations, F_C in Fig. 2b only represents that part of the C-flux that supports the water column respiration. It does not include benthic R and C burial. To scale our F_C calculations, F_C at 150 m, seaward of C8, ranged from 3 to $6\,mmol\,CO_2\,m^{-3}\,d^{-1}$ (Table 6). These fluxes are comparable to the range of 2.5 to $6.2\,mmol\,CO_2\,m^{-3}\,d^{-1}$ recently measured at 100 m in the eddy-upwelling in the South China Sea (Jiao et al., 2014).

As one would expect with strong F_C at C8, even at 1000 m, the C flux transfer efficiency (T_{eff}, Buesseler et al., 2007) at this station (19) is high and the NRE low (Table 6, Fig. 3b). T_{eff} between 150 and 500 m ($T_{eff_{500}}$) is 82 and the NRE is only 18 % (Table 6). Ironically, despite the decrease in F_C throughout the water column at C8 between 17 and 23 September, $T_{eff_{500}}$ only decreased by less than a factor of 2 to 45 % (Table 6). The impact on the NRE was greater, increasing 3 fold to 55 % (Table 6). $T_{eff_{500}}$ at other locations ranged from 28 at C10 to 47 at C14 (Fig. 3b). In addition to this unique documentation of the temporal variability of F_C from Table 5, Fig. 2b demonstrates its mesoscale spatial variability. That transect shows a maxima occurring throughout the water column, 50 km from the coast at the upper slope position, C8. As Table 5

and Fig. 3a show, the benthic R and burial are also high at this location. Figure 3b highlights the importance of the maximum curvature of the respiration-depth profile. As b increases towards 2 (absolute value) the NRE increases towards 70 % and the $T_{\text{eff}_{150-500}}$ decreases towards 30 %.

HEP in the Ez (Fig. 2d and Table 7) ranges from a high of $555\,\mathrm{J\,d^{-1}\,m^{-3}}$ at the R maximum at C5 (sta 20) to a low of $69\,\mathrm{J\,d^{-1}\,m^{-3}}$ at the bottom of the Ez at C3 (sta 21). It drops slightly over the continental slope, but further offshore over the trench (C12) high values of $880\,\mathrm{J\,d^{-1}\,m^{-3}}$ can be found (Fig. 2d). In the far offshore the Ez HEP only reaches values of $315\,\mathrm{J\,d^{-1}\,m^{-3}}$. As examples of low HEP values, at 4755 m in the trench it decreases to $0.02\,\mathrm{J\,d^{-1}\,m^{-3}}$. Thus the range of HEP by all the respiratory ETS and oxidative phosphorylation coupling in the microplankton of this part of the Peru current upwelling system spans 4 orders of magnitude from $0.02\,\mathrm{J\,d^{-1}\,m^{-3}}$ in the abyssalpelagic waters of the trench to $880\,\mathrm{J\,d^{-1}\,m^{-3}}$ in the Ez above. This is the first time such calculations have been made. Integrating the epipelagic HEP (Table 7) over the upper 150 m yields a range from a low of $6.6 \times 10^{-3}\,\mathrm{MJ\,d^{-1}\,m^{-2}}$ to a high of $0.39\,\mathrm{MJ\,d^{-1}\,m^{-2}}$, averaging $0.09\,\mathrm{MJ\,d^{-1}\,m^{-2}}$. This average HEP is only 0.7 % of the average solar radiation ($13.5 \pm 4.0\,\mathrm{MJ\,d^{-1}\,m^{-2}}$) at the C-Line sea surface between 12–24 September during the JASON-76 cruise (Packard and Jones, 1978).

5 Discussion

Here we have demonstrated the calculation of $R_{\mathrm{CO_2}}$, F_{C}, NRE, and HEP in an ocean section from microplankton ETS activity measurements. We have previously explained how ocean water column $R_{\mathrm{CO_2}}$ determines F_{C} by oxidizing sinking POC and remineralizing nutrient salts (Osma et al., 2014; Packard and Codispoti, 2007). Figure 3b shows that the maximum curvature of the respiration-depth profile determines NRE as well as F_{C} transfer efficiency. The offshore $R_{\mathrm{CO_2}}$ section (Fig. 2a) shows the variability of R with depth and location in the upwelling area and how its impact on upper mesopelagic waters is displaced seaward to C8 from the chlorophyll

Full Screen / Esc

Printer-friendly Version

Interactive Discussion

maximum at C5 (Fig. 1b). The F_C section (Fig. 2b) demonstrates the power of using R to calculate spatial variability of F_C by revealing a F_C maximum at position C8 over the continental slope west of the upwelling center (C3). The NRE section (Fig. 2c) reveals its inverse relationship to F_C as well as variability in the water column's ability to

5 retain nutrients that would not be detectable without the original ETS activity profiles. The HEP section (Fig. 2d) showing the energy production by the ATPases in microbial mitochondrion and plasmalemma membranes of bacteria and archaea in the water column is a new representation of this variable in oceanographic analysis. As expected, it reflects the R_{CO_2} section.

10 Ocean R_{CO_2} filters sinking POC and and should vary inversely with benthic R and burial. However, the relationship between the two variables is more complicated (Figs. 2a and 3a). We can see this in the R maximum 50 km off the Peru coast at C-Line position C8 (sta 19). One might expect low benthic R and C burial here, but that is not the case (Fig. 3a). From the difference between integrating the R function (Eq. 2)

15 to infinity and integrating it to the ocean bottom ($z = s$) we calculate a high level of benthic R and C burial (Fig. 3a). The minimum NRE at C-Line position, C8, in Fig. 2c explains this discrepancy. The delivery of POC to the bottom depends, not directly on F_C, but on the ratio of the water column R (Fig. 2a) to F_C (Fig. 2b). This ratio is the NRE minimum at C8 (Fig. 2c) explaining why the high POC delivery, needed to sustain the

20 high benthic R and C burial at this station, is sustained. A C-Line section of the T_{eff}, the inverse of the NRE, it would have revealed a T_{eff} maximum at C8. One can deduce this from Fig. 3b.

ETS measurements can be used, not only to calculate F_C, NRE, and HEP, but also to calculate biological heat production (Pamatmat et al., 1981), age, and flow rates of

25 deep and bottom waters (Packard, 1985). In anoxic waters, if the background chemistry (Richards, 1965) is known, ETS measurements provide proxy rate measurements for denitrification (Codispoti and Packard, 1980; Dalsgaard et al., 2012), NO_2^- production, nitrous oxide production, and sulfide production (Packard et al., 1983), and even for iron and magnesium reduction rates (Lane et al., 2010). All are different forms of

Peru upwelling plankton respiration

T. T. Packard et al.

R controlled by the same basic respiratory ETS. Furthermore, because the energy generation of nitrification is based on a variation of this ETS, its measurement is likely also a proxy for nitrification in water columns or sediments under the right chemical conditions.

5   HEP as ATP generation in the ocean water column could have been calculated from R_{O_2} since Ochoa first established the connection between ATP production and R in 1943 (Ochoa, 1943), but until now calculations of biological energy production, including HEP, in the ocean have not been made (Karl, 2014). HEP and R_{CO_2} in the Peru upwelling system have similar time and space distributions (Fig. 2a and d) even

10   though the ATP/2e⁻ relationships between oxidative phosphorylation and the rate of electron transfer in aerobic metabolism and denitrification are different. In aerobic metabolism, with NADH supplying most of the electrons to the ETS, the ATP/2e⁻ ratio is 2.5. In denitrifying microbes ATP/2e⁻ is 1.0 (van Loosdrecht et al., 1997; Smolders et al., 1994). Nevertheless, unless we were to focus only on the O_2 minimum zone, this

15   difference is not apparent.

6   Conclusions

Organic C fluxes are critical component of reliable carbon budgets, but they are so difficult to measure that rarely can enough measurements be amassed to construct a synoptic section of F_C. Here, from plankton respiration models we present an original

20   mode of calculating F_C sections as well as benthic respiration and carbon burial. Furthermore, we reveal the importance of plankton respiration in determining the capacity of a plankton community in retaining water column nutrients. In this light, we develop the concept of nutrient retention efficiency (NRE) demonstrating its variability in an ocean section. In addition, we show that the curvature of the respiration profile

25   controls both the NRE and F_C. Finally, we use respiration to model the heterotrophic energy production of plankton metabolism and find it to be, as expected, a small fraction of the solar energy input.

References

Alberty, R. and Goldberg, R.: Standard thermodynamic formation properties of adenosie 5′-triphosphate series, Biochemistry, 31, 10610–10615, 1992. 16184

Barber, R., Huntsman, S., Kogelschatz, J., Smith, W., and Jones, B.: Coastal Upwelling Ecosystems Analysis, Data Report 49, Carbon, Chlorophyll and Light Extinction from JOINT II, vol. 49, CUEA Data Rep, Duke University, Beaufort, NC, USA, 1978. 16181, 16182

Buesseler, K. and Boyd, P.: Shedding light on precesses that control particle export and flux attenuation in the twilight zone of the open ocean, Limnol. Oceanogr., 54, 1210–1232, 2009. 16180

Buesseler, K., Lamborg, C., Boyd, P., Lam, P., Trull, T., Bidigare, R., Bishop, J., Casciotti, K., Dehairs, F., Elskens, M., Honda, M., Karl, D., Siegel, D., Silver, M., Steinberg, D., Valdes, J., Van Mooy, B., and Wilson, S.: Revisiting carbon flux through the ocean's twilight zone, Science, 316, 567–570, 2007. 16180, 16187, 16201

Burd, A., Hansell, D., Steinberg, D., Anderson, T., Arístegui, J., Baltar, F., Beaupré, S., Buesseler, K., Dehairs, F., Jackson, G., Kadko, D., Koppelmann, R., Lampitt, R., Nagata, T., Reinthaler, T., Robinson, C., Robison, B., Tamburini, C., and Tanaka, T.: Assessing the apparent imbalance between geochemical and biochemical indicators of meso- and bathypelagic biological activity What the @$?! is wrong with present calculations of carbon budgets?, Deep-Sea Res. Pt. II, 57, 1557–1571, 2010. 16179

Charland, M.: SigmaPlot 2000/2001 for Scientists, Riparian House, Merrickville (Ontario), 2002. 16183

Discussion Paper | Discussion Paper | Discussion Paper | Discussion Paper |

BGD

11, 16177–16206, 2014

Peru upwelling plankton respiration

T. T. Packard et al.

Title Page

Abstract | Introduction

Conclusions | References

Tables | Figures

◀ | ▶

◀ | ▶

Back | Close

Full Screen / Esc

Printer-friendly Version

Interactive Discussion

Codispoti, L. and Packard, T.: Denitrification rates in the eastern tropical South Pacific, J. Mar. Res., 38, 453–477, 1980. 16182, 16186, 16189, 16197

Codispoti, L., Brandes, J., Christensen, J., Devol, A., Naqvi, S., Paerl, H., and Yoshinari, T.: The oceanic fixed nitrogen and nitrous oxide budgets: moving targets as we enter the anthropocene?, Sci. Mar., 65, 85–105, 2001. 16182

Craig, H.: The deep metabolism: oxygen consumption in abyssal ocean water, J. Geophys. Res., 76, 5078–5086, 1971. 16183

Dalsgaard, T., Thamdrup, B., Farías, L., and Revsbech, N.: Anammox and denitrification in the oxygen minimum zone of the eastern South Pacific, Limnol. Oceanogr., 57, 1331–1346, 2012. 16182, 16186, 16189

Ducklow, H. and Doney, S.: What is the metabolic state of the oligotrophic ocean? A debate, Annu. Rev. Mar. Sci., 5, 525–533, 2013. 16179

Ferguson, S.: ATP synthase: From sequence to ring size to the P/O ratio, P. Natl. Acad. Sci. USA, 107, 16755–16756, 2010. 16180, 16184

Fernández, C., Faría, L., and Alcaman, M.: Primary production and nitrogen regeneration processes in surface waters of the Peruvian upwelling system, Prog. Oceanogr., 83, 159–168, 2009. 16181

Fernández-Urruzola, I., Osma, N., Packard, T., Gómez, M., and Postel, L.: Distribution of zooplankton biomass and potential metabolic activities across the northern Benguela upwelling system, J. Marine Syst., doi:10.1016/j.jmarsys.2014.05.009, online first, 2014. 16186

Garfield, P., Packard, T. T., and Codispoti, L.: Particulate protein in the Peru upwelling system, Deep-Sea Res., 26, 623–639, 1979. 16182

Giering, S., Sanders, R., Lampitt, R., Anderson, T., Tamburini, C., Boutrif, M., Zubkov, M., Marsay, C., Henson, S., Saw, K., Cook, K., and Mayor, D.: Reconciliation of the carbon budget in the ocean's twilight zone, Nature, 507, 480–483, doi:10.1038/nature13123, 2014. 16179

Gruber, N. and Sarmiento, J.: Global patterns of marine nitrogen fixation and denitrification, Global Biogeochem. Cy., 11, 235–266, 1997. 16183

Hafferty, A., Codispoti, L., and Huyer, A.: JOINT-II R/V *Melville* Legs I, II and IV WV Iselin Leg II bottle data March 1977–May 1977, 45, CUEA Data Rep, Oregon State University, Corvallis, OR, USA, 1978. 16182

Odum, H. T.: Primary production in flowing waters, Limnol. Oceanogr., 1, 102–117, 1956. 16180

Jiao, N., Zhang, Y., Zhou, K., Li, Q., Dai, M., Liu, J., Guo, J., and Huang, B.: Revisiting the CO_2 "source" problem in upwelling areas – a comparative study on eddy upwellings in the South China Sea, Biogeosciences, 11, 2465–2475, doi:10.5194/bg-11-2465-2014, 2014. 16187

Karl, D. M.: Solar Energy capture and transformation in the sea, Elementa: Science of the Anthropocene, 2, 1–6, doi:10.12952/journal.elementa.000021#sthash.UJseSxIf.dpuf, 2014. 16180, 16190

Kenner, R. and Ahmed, S.: Measurements of electron transport activity in marine phytoplankton, Mar. Biol., 33, 119–127, 1975. 16182

King, L.: The coastal upwelling ecosystems analysis program as an experience in international cooperation, Ocean Dev. Int. Law, 9, 269–288, 1981. 16181

Kogelshatz, J., Shepherd, R., Whitledge, T., Codispoti, L., and Huyer, A.: JOINT-II JASON 76 hydro data. R/V *EASTWARD* Cruises E-5F-76 through E-5L-76, vol. 38, International Decade of Ocean Exploration, CUEA Data Rep, Oregon State University, Corvallis, OR, USA, 1978. 16181, 16182, 16196

Lane, N., Allen, J., and Martin, W.: How did LUCA make a living? Chemiosmosis in the origin of life, BioEssays, 32, 271–280, 2010. 16180, 16189

Laufkötter, C., Vogt, M., and Gruber, N.: Long-term trends in ocean plankton production and particle export between 1960–2006, Biogeosciences, 10, 7373–7393, doi:10.5194/bg-10-7373-2013, 2013. 16179

Lotka, A.: Elements of Physical Biology, Williams & Wilkins Company, Baltimore, 1925. 16180

Moran, L., Horton, R., Scrimgeour, K., and Perry, M.: Principles of Biochemistry, Pearson/Prentice Hall, Upper Saddle River, NJ, USA, 2012. 16184

Ochoa, S.: Efficiency of aerobic phosphorylation in cell-free heart extracts, J. Biol. Chem., 151, 493–505, 1943. 16190

Osma, N., Fernández-Urruzola, I., Packard, T., Postel, L., Gómez, M., and Pollehne, F.: Short-term patterns of vertical particle flux in northern Benguela: a comparison between sinking POC and respiratory carbon consumption, J. Marine Syst., doi:10.1016/j.jmarsys.2014.01.004, online first, 2014. 16179, 16183, 16186, 16188

Packard, T.: Organizers Remarks: Coastal Upwelling. Coastal and Estuarine Sciences 1, vol. xi–xiii, edited by: Richards, F. A., American Geophysiscal Union, Wasington DC, 1981. 16181

Packard, T.: Oxygen consumption in the ocean: measuring and mapping with enzyme analysis, in: Mapping Strategies in Chemical Oceanography, American Chemical Society, Washington, DC, 177-209, 1985. 16189

Packard, T. and Christensen, J.: Respiration and vertical carbon flux in the Gulf of Maine water column, J. Mar. Res., 62, 93–115, 2004. 16179, 16182, 16183, 16186, 16197

Packard, T. and Codispoti, L.: Respiration, mineralization, and biochemical properties of the particulate matter in the southern Nansen Basin water column in April 1981, Deep-Sea Res. Pt. I, 54, 403–414, 2007. 16186, 16188

Packard, T. and Gómez, M.: Modeling vertical carbon flux from zooplankton respiration, Prog. Oceanogr., 110, 59–68, 2013. 16179, 16183, 16184

Packard, T. and Jones, V.: Biochemistry and ecology of the Peru Current: the JASON expedition to the Peru upwelling system, September 1976, CUEA Tech Rep, Bigelow Laboratory, Boothbay Harbor, MW, USA, 46, 129, 1978. 16181, 16182, 16188, 16196

Packard, T., Healy, M., and Richards, F.: Vertical distribution of the activity of the respiratory electron transport system in marine plankton, Limnol. Oceanogr., 16, 60–70, 1971. 16182

Packard, T., Garfield, P., and Codispoti, L.: Oxygen Consumption and Denitrification Below the Peruvian Upwelling. Coastal Upwelling: Its Sediment Record, vol. 147–173, edited by: Suess, E. and Thiede, J., Plenum Press, New York, 1983. 16189

Pamatmat, M., Graf, G., Bengtsson, W., and Novak, C.: Heat production, ATP concentration and electron transport activity of marine sediments, Mar. Ecol. Prog. Ser., 4, 135–143, 1981. 16189

Richards, F.: Coastal Upwelling, American Geophysical Union, Washington DC, 529 pp., 1981. 16181

Richards, F. A.: Anoxic Basins and Fjords. Chemical Oceanography, edited by: Riley, J. P. and Skirrow, G., Academic Press, New York, 1965. 16189

Barber, R. T., Dugdale, R. C., MacIsaac, J. J., and Smith, R. L.: Variations in phytoplankton growth associated with the source and conditioning of upwelling water, Invest Pesqu, 35, 171–193, 1971.

Ryther, J. H., Menzel, D. W., Hulburt, E. M., Lorenzen, C. J., and Corwin, N.: Production and utilization of organic matter in the Peru Coastal Current, Woods Hole Oceanographic Institution, Woods Hole, MA, USA, WHOI technical reports, 35, 34–60, 1971. 16181

Santoso, A., McGregor, S., Jin, F., Cai, W., England, M., An, S., McPhaden, M., and Guilyardi, E.: Late-twentieth-century emergence of the El Niño propagation asymmetry and future projections, Nature, 504, 126–130, 2013. 16179

Smolders, G., van der Meij, J., van Loosdrecht, M. C., and Heijnen, J. J.: Stoichiometric model of the aerobic metabolism of the biological phosphorus removal process, Biotech. Bioeng., 44, 837–848, 1994. 16185, 16190

Suess, E.: Particulate organic carbon flux in the oceans-surface productivity and oxygen utilization, Nature, 288, 260–263, 1980. 16179

Takahashi, T., Broecker, W., and Langer, S.: Redfield ratio based on chemical data from isopycnal surfaces, J. Geophys. Res., 90, 6907–6924, 1985. 16186

van Loosdrecht, M. C. M., Smolders, G. J., Kuba, T., and Heijnen, J. J.: Metabolism of micro-organisms responsible for enhanced biological phosphorus removal from wastewater, Antonie Leeuwenhoek, 71, 109–116, 1997. 16185, 16190

Walker, J.: ATP synthesis by rotary catalysis, Angew. Chem. Int. Ed., 37, 2308–2319, 1998. 16180

Watt, N., Montgomery, M., Runswick, M., Leslie, A., and Walker, J.: Bioenergetic cost of making an adenosine triphosphate molecule in animal mitochondria, P. Natl. Acad. Sci. USA, 107, 16823–16827, doi:10.1073/pnas.1011099107, 2010. 16180

Williams, P., Quay, P., Westberry, T., and Behrenfeld, M.: The oligotrophic ocean is autotrophic, Annu. Rev. Mar. Sci., 5, 535–549, 2012. 16179

Wooster, W.: Yearly changes in the Peru Current, Limnol. Oceanogr., 6, 222–226, 1961. 16181

Wyrtki, K.: Circulation and water masses in the Eastern equatorial Pacific Ocean, Int. J. Oceanol. Limnol., 1, 117–147, 1967. 16181

Table 1. Oceanographic characteristics of Peru upwelling C-Line stations during Duke University's JASON-76 R/V *Eastward* cruise E-5H-67. Ez depth is the 1 % light level. Original data are in CUEA Data Reports (Kogelshatz et al., 1978; Packard and Jones, 1978).

CUEA C-Line Position (JASON Station)	Coordinates	Date in Sep 1976	Distance to coast (km)	Ocean depth (m)	Surface temperature (°C)	Surface salinity (PSU)	Euphotic zone (m)	Surface chlorophyll (mg m^{-3})	Surface respiration (µmol O$_2$ m^{-3} h^{-1})	Surface net productivity (mg C m^{-3} h^{-1})
C1 (22)	15°03.2′ S 75°26.0′ W	20	2.7	63	14.28	34.902	24	3.06	56.11	6.84
C3 (15)	15°05.9′ S 75°31.4′ W	12	12.9	117	14.26	–	42	2.09	24.11	3.67
C3 (21)	15°06.5′ S 75°31.0′ W	19	12.9	120	14.10	34.869	33	3.67	83.99	8.08
C5 (20)	15°09.9′ S 75°35.7′ W	18	24.7	500	15.59	34.921	21	6.96	119.13	18.24
C5 (37)	15°10.5′ S 75°36.2′ W	24	24.7	607	15.00	34.921	27	3.77	79.97	8.88
C8 (19)	15°16.9′ S 75°47.8′ W	17	49.9	1880	14.97	34.902	29	4.11	80.32	9.65
C8 (36)	15°16.9′ S 75°14.8′ W	23	49.9	2150	16.10	35.069	29	3.90	87.67	12.35
C10 (18)	15°22.0′ S 75°59.8′ W	16	70.9	4300	15.92	35.077	36	1.06	34.35	1.64
C12 (17)	15°28.0′ S 76°08.0′ W	15	92.6	4000	15.75	35.046	40	1.14	47.14	1.93
C12 (35)	15°29.0′ S 76°07.8′ W	22	92.6	4755	15.46	34.950	21	7.47	144.71	16.64
C14 (16)	15°55.8′ S 76°51.6′ W	13	185.2	2680	16.48	35.147	43	0.92	40.90	1.63

Table 2. Step-by-step calculations of F_C from ETS activity at C-Line position C12 (station 35). Potential R (Φ), R_{O_2}, N_2 production from denitrification (R_{N_2}) and respiratory CO_2 production (R_{CO_2}) were first determined from temperature-corrected ETS activity values. Φ is stoichiometrically related to electrons by a factor of 4 ($O_2 + 4e^- + 4H^+ \rightarrow 2H_2O$). R_{O_2} is 0.26 of Φ (Packard and Christensen, 2004). R_{N_2} relates to ETS activity according to Codispoti and Packard (1980). Here, denitrifying waters occur between 93 and 233 m (values in bold). R_{CO_2} was calculated from both R_{O_2} and R_{N_2} (see Sect. 2). Column 7 shows the modeled R_{CO_2} values below the R maximum (13 m), obtained from the depth-normalized power function ($R_{CO_2} = R_m(z/z_m)^b$) fitted to the data in Column 6. F_C was determined by integrating either to the bottom (F_{t-s}, Column 8) or to infinity (F_∞, Column 9). The first represents the C consumed by R from the Ez (21 m) to the bottom, while the second includes benthic R and C burial. The difference between F_∞ and F_{t-s} equals benthic R and the C burial rate (Column 10). Column 11 represents the C flux determined by trapezoidal approximation, which relates to F_{t-s} by the regression: $F_{t-s} = 0.85F_{c_{trap}} - 0.54$ ($r^2 = 0.99$, $p < 0.001$).

Depth z (m)	ETS Activity (neq min⁻¹ L⁻¹)	Φ (µmol O_2 h⁻¹ m⁻³)	R_{O_2} (µmol O_2 h⁻¹ m⁻³)	R_{N_2} (µmol N_2 h⁻¹ m⁻³)	R_{CO_2} (µmol CO_2 h⁻¹ m⁻³)	R_{CO_2} modeled (µmol CO_2 d⁻¹ m⁻³)	F_C to bottom F_{t-s} (mmol C d⁻¹ m⁻²)	F_C to infinity F_∞ (mmol C d⁻¹ m⁻²)	Benthic respiration and burial $F_\infty - F_{t-s}$	C-Flux to bottom Trap Calc (mmol C d⁻¹ m⁻²)
0.5	37.10	556.56	144.71	–	102.74	–	–	–	–	–
3	37.81	567.14	147.46	–	104.69	–	–	–	–	–
5	35.69	535.39	139.20	–	98.83	–	–	–	–	–
9	33.65	504.68	131.22	–	93.16	–	–	–	–	–
13	39.19	587.87	152.85	–	108.52	1629.67	–	–	–	–
21	15.34	230.16	59.84	–	42.49	707.39	19.71	20.07	0.36	25.49
31	8.79	131.81	34.27	–	24.33	359.18	14.68	15.04	0.36	20.16
93	**0.44**	–	–	**0.25**	**0.44**	53.09	6.31	6.67	0.36	7.38
233	**0.35**	–	–	**0.20**	**0.35**	10.74	3.02	3.38	0.36	3.38
465	0.05	0.75	0.19	–	0.14	3.23	1.66	2.03	0.36	1.76
698	0.01	0.14	0.04	–	0.03	1.59	1.14	1.50	0.36	1.20
930	0.02	0.23	0.06	–	0.04	0.97	0.85	1.21	0.36	0.90
1395	0.01	0.21	0.05	–	0.04	0.48	0.54	0.90	0.36	0.57
1860	0.01	0.13	0.04	–	0.02	0.29	0.36	0.73	0.36	0.40
4755	–	–	–	–	–	0.06	0	0.36	0.36	0

Discussion Paper | Discussion Paper | Discussion Paper | Discussion Paper |

BGD

11, 16177–16206, 2014

Peru upwelling plankton respiration

T. T. Packard et al.

Title Page

Abstract | Introduction

Conclusions | References

Tables | Figures

|◄ | ►|

◄ | ►

Back | Close

Full Screen / Esc

Printer-friendly Version

Interactive Discussion

Table 3. R_{O_2} as $\mu mol\,O_2\,h^{-1}\,m^{-3}$ profiles in the microplankton along the C-line section in September 1976. In the OMZ depths (values in bold), NO_3^- was the electron donor and N_2 was produced during denitrification (R_{N_2} as $\mu mol\,N_2\,h^{-1}\,m^{-3}$). C-Line position as well as JASON station number (parenthesis) are given. Depth (z) is in meters and R refers to either R_{O_2} or R_{N_2} depending on the shading. Calculations are explained in the text.

C1 (22)		C3 (15)		C3 (21)		C5 (20)		C5 (37)		C8 (19)		C8 (36)		C10 (18)		C12 (17)		C12 (35)		C14 (16)	
z(m)	R	z(m)	R	z(m)	R	z(m)	R	z(m)	R	z(m)	R	z(m)	R	z(m)	R	z(m)	R	z(m)	R	z(m)	R
0.5	56.11	0.5	24.11	0.5	83.99	0.5	119.13	0.5	79.97	0.5	80.32	0.5	87.67	0.5	34.35	0.5	47.14	0.5	144.71	0.5	40.90
4	84.66	6	34.89	5	78.92	3	154.77	4	86.75	4	92.40	5	97.89	5	35.79	6	30.65	3	147.46	7	34.62
6	44.15	9	35.86	9	64.26	6	130.83	7	95.81	8	75.17	8	88.41	8	51.17	16	29.04	5	139.20	11	36.09
10	71.05	17	42.74	14	43.68	9	180.26	11	86.29	12	54.66	12	83.74	15	40.07	26	34.38	9	131.22	18	54.67
16	60.88	28	30.99	21	20.57	14	97.08	17	77.46	19	69.74	19	63.75	24	87.36	40	29.61	13	152.85	28	44.78
24	42.41	42	15.42	33	12.05	21	41.27	27	67.29	29	45.27	29	19.16	36	24.75	**233**	**0.09**	21	59.84	43	25.66
				47	**3.15**	**93**	**0.48**	40	71.55	**93**	**1.12**	44	18.08	**233**	**0.16**			31	34.27	100	4.51
				93	**1.80**	**233**	**0.67**			**233**	**0.48**	**93**	**0.59**	465	0.04			**93**	**0.25**	250	0.73
						465	**0.09**			465	0.62	**233**	**0.15**	1860	0.02			**233**	**0.20**	500	0.22
										930	0.36	465	0.04					465	0.19	750	0.11
										1395	0.22	698	0.03					698	0.04	1000	0.06
												930	0.05					930	0.06	2000	0.09
												1395	0.06					1395	0.05		
																		1860	0.04		

BGD

11, 16177–16206, 2014

Peru upwelling
plankton respiration

T. T. Packard et al.

Title Page

Abstract | Introduction

Conclusions | References

Tables | Figures

◄◄ | ►►

◄ | ►

Back | Close

Full Screen / Esc

Printer-friendly Version

Interactive Discussion

Table 4. Power functions for microplankton R (mmol CO_2 d^{-1} m^{-3}) as functions of normalized depth, $R_{CO_2} = R_m(z/z_m)^b$, where R_{CO_2} is the respiratory CO_2 production at any depth (z), R_m is the R maximum (mmol CO_2 d^{-1} m^{-3}) in the water column, z/z_m is the depth normalized by the depth at R_m, and b is the maximum curvature of the power function. Both z/z_m and b are unitless. Δz represents the depth range of the R values considered. The table includes the r^2 from the least-square regression analysis of the R models (Sigma Plot vs. 12.5) and the number of data considered (n). The significance level of the regressions is indicated by superscript letters, a, b, and c. The last four columns represent the linear regression of the respiration-model verification analysis. The slope, the intercept and the r^2 are given. The n value for each verification analysis is the same as the n used for each R model (column 7). These R models are based on ETS activity data taken during R/V *Eastward* JASON-76 expedition, along the C-Line.

CUEA C-Line Position (JASON Station)	Δz (m)	z_m (m)	R_m (mmol CO_2 d^{-1} m^{-3})	b	r^2	n	Modeled vs. Calculated R_{CO_2}			
							slope	intercept	r^2	n
C1 (22)	4–24	4	1.538	−0.355	0.864	4	0.975	25.24	0.878	4
C3 (15)	17–42	17	0.783	−1.109	0.929	3	1.041	20.42	0.926	3
C3 (21)	5–93	0.5	20.659	−1.080	0.972[c]	7	1.095	45.37	0.905[b]	7
C5 (20)	9–465	9	2.796	−1.655	0.951[b]	6	0.890	4.25	0.996[b]	6
C5 (37)	7–40	7	1.596	−0.192	0.873[a]	5	0.875	168.87	0.902[a]	5
C8 (19)	4–1395	4	3.247	−1.168	0.957[c]	10	1.348	129.78	0.686[a]	10
C8 (36)	5–1395	5	4.413	−1.670	0.949[c]	12	0.937	−44.14	0.808[b]	12
C10 (18)	24–1860	24	0.946	−2.051	0.962[a]	5	0.638	29.3	0.976[a]	5
C12 (17)	0.5–233	0.5	3.172	−0.720	0.497	7	2.596	−661.42	0.339	7
C12 (35)	13–1860	13	1.630	−1.740	0.948[c]	10	0.627	10.56	0.998[b]	10
C14 (16)	18–2000	18	1.183	−1.624	0.968[c]	9	1.043	−19.72	0.910[b]	9

[a] $p < 0.05$
[b] $p < 0.001$
[c] $p < 0.0001$

Table 5. Microplankton respiration in epipelagic, mesopelagic, and bathypelagic waters along the C-Line across the Peru Current upwelling system at 15° S. Calculations are based on the R models in Table 4. Shoreward of C5 the bottom limits the lower depth boundary. Note the 1000-fold shift in the rates expressed per area (columns 3–7) and per volume (columns 8–10).

CUEA C-Line Position (JASON station)	Ocean depth (m)	Water column R (mmol C m^{-2} d^{-1})	Benthic respiration and C burial (mmol C m^{-2} d^{-1})	Epipelagic 1–150 m (mmol C m^{-2} d^{-1})	Mesopelagic 150–1000 m (mmol C m^{-2} d^{-1})	Bathypelagic 1000 m–bottom (mmol C m^{-2} d^{-1})	Epipelagic 1–150 m (µmol C m^{-3} d^{-1})	Mesopelagic 150–1000 m (µmol C m^{-3} d^{-1})	Bathypelagic 1000 m–bottom (µmol C m^{-3} d^{-1})
C1 (22)	63	53.98	–	53.98	–	–	856.85	–	–
C3 (15)	117	80.32	99.23	80.32	–	–	686.50	–	–
C3 (21)	120	45.81	82.99	45.81	–	–	381.75	–	–
C5 (20)	550	252.48	2.60	248.99	3.49	–	1659.96	8.72	–
C5 (37)	607	507.91	–	162.98	344.93	–	1086.51	754.78	–
C8 (19)	1880	82.10	27.37	67.58	11.46	3.07	450.51	13.48	3.49
C8 (36)	2150	153.46	0.57	150.65	2.43	0.38	1004.36	2.85	0.33
C10 (18)	4300	1256.23	0.09	1262.18	2.72	0.34	8414.54	3.20	0.10
C12 (17)	4000	64.36	–	22.28	19.57	22.51	148.55	23.02	7.50
C12 (35)	4755	318.83	0.36	314.51	3.53	0.79	2096.75	4.16	0.21
C14 (16)	2680	318.14	1.50	310.56	6.30	1.28	2070.43	7.41	0.76

Table 6. Carbon flux models F_C at C-Line positions deeper than 500 m in the Peru Upwelling System Sep 1976. From these models, F_C at four different depths were determined. NRE and F_C Transfer Efficiency (T_{eff}) for the upper mesopelagic waters (150–500 m) are also given. NRE was calculated as $100 \cdot R_{CO_2}/F_{c_{150}}$, where the R_{CO_2} represents the integrated R between 150 and 500 m; T_{eff} was calculated as $100 \cdot F_{c_{500}}/F_{c_{150}}$ according to Buesseler et al. (2007).

CUEA C-Line Position (JASON Station)	Ocean depth (m)	Euphotic zone, z_e (m)	F_C models	F_C from z_e (mmol C m^{-2} d^{-1})	F_C from 150 m (mmol C m^{-2} d^{-1})	F_C from 500 m (mmol C m^{-2} d^{-1})	F_C from 1000 m (mmol C m^{-2} d^{-1})	NRE 150–500 m (%)	Teff 150–500 m (%)
C5 (20)	550	21	$22.07\,(z/z_e)^{-0.655}$	22.07	6.09	2.77	–	54.6	45.4
C8 (19)	1880	29	$55.25\,(z/z_e)^{-0.168}$	55.25	41.92	34.24	30.48	18.3	81.7
C8 (36)	2150	29	$10.14\,(z/z_e)^{-0.670}$	10.14	3.37	1.51	0.95	55.4	44.6
C10 (18)	4300	36	$14.11\,(z/z_e)^{-1.051}$	14.11	3.15	0.89	0.43	71.8	28.2
C12 (35)	4755	21	$20.07\,(z/z_e)^{-0.740}$	20.07	4.68	1.92	1.15	59.0	41.0
C14 (16)	2680	43	$19.80\,(z/z_e)^{-0.624}$	19.80	5.81	2.74	1.78	52.8	47.2

Table 7. HEP as ATP production in epipelagic, mesopelagic, and bathypelagic waters of the C-Line section, September 1976. Shoreward of C5 the bottom limits the lower depth boundary.

CUEA C-Line Location (JASON station)	Ocean depth (m)	Epipelagic HEP 1–150 m ($J m^{-3} d^{-1}$)	Mesopelagic HEP 150–1000 m ($J m^{-3} d^{-1}$)	Bathypelagic HEP 1000 m-bottom ($J m^{-3} d^{-1}$)
C1 (22)	63	289.63	–	–
C3 (15)	117	232.05	–	–
C3 (21)	120	173.40	–	–
C5 (20)	550	977.93	1.19	–
C5 (37)	607	367.24	255.11	–
C8 (19)	1880	138.77	3.59	0.89
C8 (36)	2150	319.41	0.80	0.09
C10 (18)	4300	2609.16	0.89	0.03
C12 (17)	4000	43.60	4.56	1.23
C12 (35)	4755	535.98	1.18	0.06
C14 (16)	2680	699.88	2.51	0.26

Figure 1. (a) C-line section orthogonal to the Peru coast at 15° S. The innermost C-Line position, C1, was 2.7 km from the coast between Cabo Nazca and Punta Santa Ana. The outermost position, C14, was located west of the Peru-Chili trench 185.2 km from the coast. Depth along this transect ranged from 63 m at C1 to 4755 m at C12. C14 was in 2680 m of water on the gently rising abyssal plain seaward of the trench (inset upper left). **(b)** Density (σ_t), NO_3^- (µM units) and phytoplankton chlorophyll (mg m^{-3}) sections along the C-line from C1 to C14 (top, middle and bottom panels, respectively). All sections represent the upwelling from 13 to 20 September 1976. Scale brakes avoid interpolation over a 90 km data gap. The high phytoplankton biomass over the shelf break occurs between C5 and C8, 15 to 35 km from the coast. **(c)** NO_3^-, NO_2^-, and O_2 depth profiles through the mesopelagic waters over the Trench at C12 (top) and over the outermost station at C14 (bottom). The vertical plot at C12 documents the first step in denitrification (shaded area), NO_3^- reduction to NO_2^-, at the foot of the oxycline, in the OMZ between 150 and 300 m. In contrast, the vertical profiles at C14, 185 km off the coast, show the absence of denitrification in mesopelagic waters.

Full Screen / Esc

Printer-friendly Version

Interactive Discussion

Discussion Paper | Discussion Paper | Discussion Paper | Discussion Paper |

BGD

11, 16177–16206, 2014

Peru upwelling plankton respiration

T. T. Packard et al.

Title Page

Abstract | Introduction

Conclusions | References

Tables | Figures

|◀ | ▶|

◀ | ▶

Back | Close

Full Screen / Esc

Printer-friendly Version

Interactive Discussion
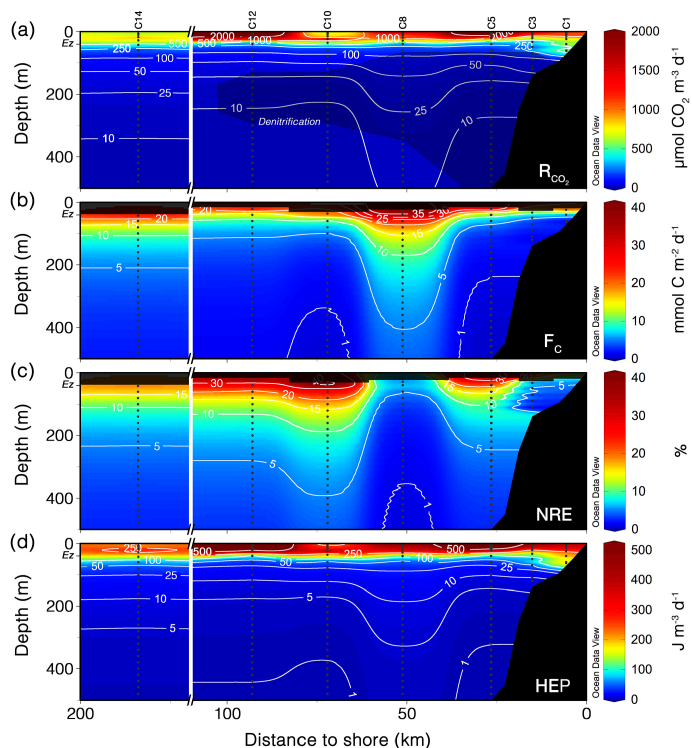
Figure 2. Sections for the upper 500 m along the C-line. **(a)** R_{CO_2}; the dark shadow delimits denitrification in the OMZ. Above the Ez, R_{CO_2} is calculated directly from ETS activity, below R_{CO_2} is determined from equations in Table 4. **(b)** F_C is calculated by the definite integral from the bottom of the euphotic zone to the ocean bottom using the R_{CO_2} models from Table 4, according to the Eqs. (2) and (3). **(c)** NRE is determined from models in Tables 4 and 6 as $100 \cdot (R_{CO_2}/F_C)$. **(d)** HEP is either derived directly from ETS activity in the surface waters or from modeled R_{O_2} or R_{N_2} below the Ez (see Sect. 2).
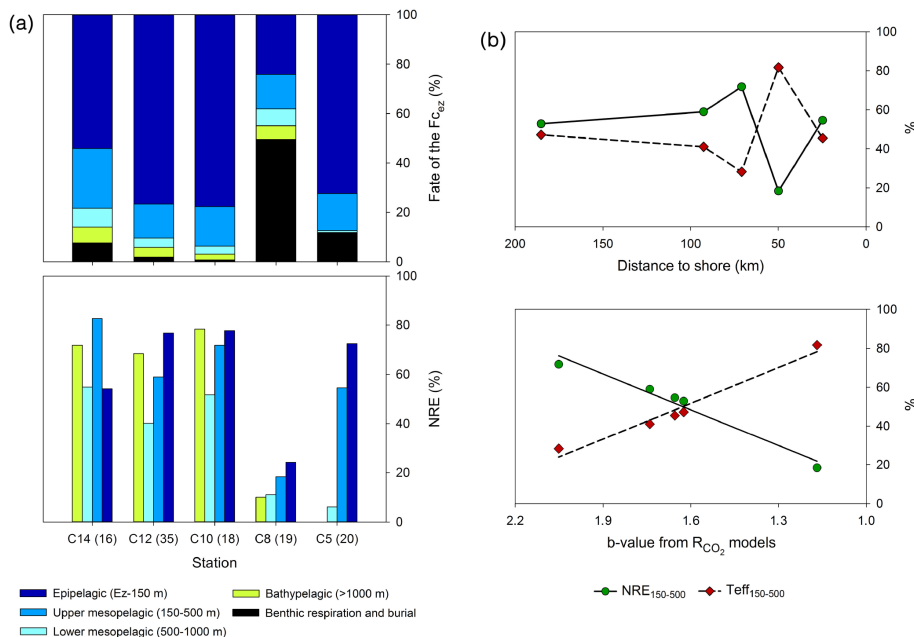
Figure 3. (a) Fate of the C fluxing out of the Ez (Fc$_{ez}$) into the water column and seafloor below (as a % of the total flux) along the C-Line (top panel). In the water column, the C is remineralized through R. In the benthos, part is remineralized and returned to the water column above and part is buried. Bottom panel shows the different efficiencies with which C is remineralized through R in 4 different zones of the water column along the C-Line. **(b)** Top panel: variability of the NRE and the T_{eff} in the upper mesopelagic waters (150–500 m) along the C-line. Bottom panel: NRE and T_{eff} as a function of the maximum curvature **(b)** (absolute value) in the R_{CO_2} models from Table 4.